ACS OMEGA

Open Access

http://pubs.acs.org/journal/acsodf

Article

$CuCl_2$-Activated Sustainable Microporous Carbons with Tailorable Multiscale Pores for Effective CO_2 Capture

Shunyang Yao,[#] Zhi Li,[#] Zhen Liu, Xiaodong Geng, Li Dai,[*] and Yanmei Wang[*]

Cite This: *ACS Omega* 2023, 8, 41641−41648

Read Online

ACCESS | Metrics & More | Article Recommendations | Supporting Information

ABSTRACT: Porosity is the key factor in determining the CO_2 capture capacity for porous carbon-based adsorbents, especially narrow micropores of less than 1.0 nm. Unfortunately, this desired feature is still a great challenge to tailor micropores by an effective, low-corrosion, and environmentally friendly activating agent. Herein, we reported a suitable dynamic porogen of $CuCl_2$ to engineer microporous carbons rich in narrow micropores of <1.0 nm for solving the above problem. The porosity can be easily tuned by varying the concentration of the $CuCl_2$ porogen. The resultant porous carbons exhibited a multiscale micropore size, high micropore volume, and suitable surface nitrogen doping content, especially high-proportioned ultromicropores of <0.7 nm. As adsorbents for capturing CO_2, the obtained microporous carbons possess satisfactory CO_2 uptake, moderate heat of CO_2 adsorption, reasonable CO_2/N_2 selectivity, and easy regeneration. Our work proposes an alternative way to design porous carbon-based adsorbents for efficiently capturing CO_2 from the postcombustion flue gases. More importantly, this work opens up an almost-zero cost and industrially friendly route to convert biowaste into high-added-value adsorbents for CO_2 capture in an industrial practical application.

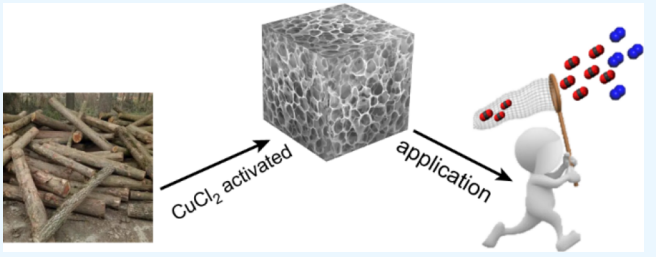

1. INTRODUCTION

The rapid and continued economic development causes a much-needed demand for energy. The combustion of large-scale fossil fuels has been continuously increasing to meet the energy requirement of the world, which brings huge CO_2 emissions. Consequently, an ever-increasing buildup of excessive CO_2 concentration in the atmosphere has been witnessed. CO_2 is one of the predominant greenhouse gases, resulting in global warming and anthropogenic climate change. Many countries have taken active measures to curb CO_2 emissions and have put forward the goal of net-zero emission.[1−3] However, it is an irresistible difficulty to totally eliminate fossil fuel combustion to supplement clean energy during the transition to net-zero emissions. In this context, CO_2 capture and storage (CCS) has been regarded as a highly promising strategy for mitigating the atmospheric CO_2 concentration and the deleterious effects of excessive CO_2 emission.[4−6]

Among the different CO_2 CCS strategies, pressure swing adsorption of CO_2 with porous solid materials is the most effective route for CO_2 capture owing to the low energy consumption, high adsorption efficiency, and facile operating conditions.[7−9] Among porous solid adsorbents, porous carbons are considered as good candidates for industrially mature CO_2 capture in large-scale practical application by virtue of large surface area, easy-to-design pore size, tunable surface chemistry, controllable morphology, low cost, easy regeneration, and wide availability.[10−14] Among these factors, pore size is the key parameter in determining the CO_2 adsorption capacity of porous carbons, which plays a decisive role in CO_2 capture capacity.[15,16] Particularly, micropores of less than 1.0 nm have a major contribution to CO_2 capacity at low pressure and high temperature for the postcombustion capture.[17] Therefore, such desirable properties have been targeted in rationally engineering porous carbons by tailoring porosity.

For this purpose, significant progress has been made in the design of such porous carbons regarding pore structure engineering by different synthesis strategies with all kinds of carbon sources. Activation technologies are the most widely adopted routes to construct porous carbons with rich porosity, especially chemical activation. On this regard, a wide variety of activating agents have been explored for chemical activation to produce well-developed pore structure, such as KOH, NaOH, $ZnCl_2$, H_3PO_4, H_2SO_4, and K_2CO_3.[18−23] Among them, KOH is the most widely used, which can efficiently contribute to generate porous carbons with high-proportioned micropores or small mesopores.[24,25] However, rich micropores can be produced in carbon skeleton and usually deliver poor control

Received: August 8, 2023
Revised: October 11, 2023
Accepted: October 16, 2023
Published: October 26, 2023

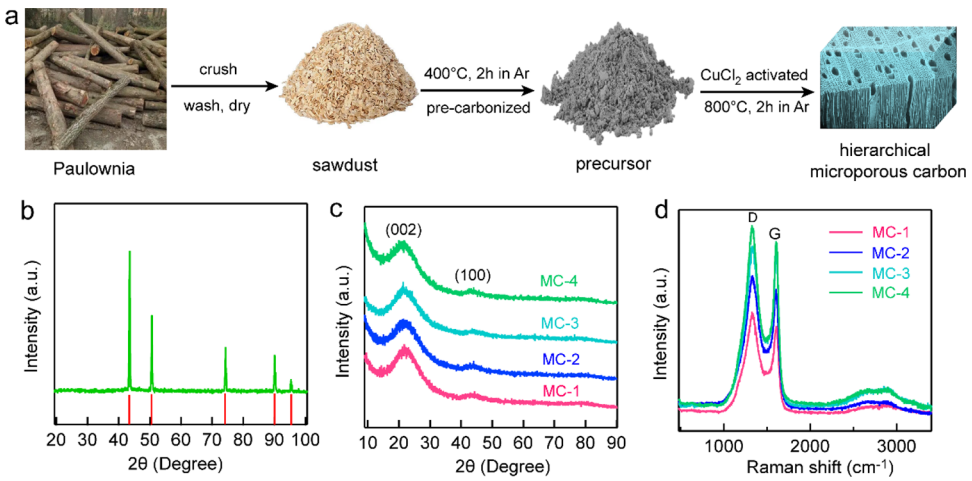

Figure 1. (a) Schematic illustration for the synthesis of MC-*x*. The XRD patterns of before (b) and after (c) acid washing and MC-*x* samples. (d) Raman spectra of MC-*x* samples.

on the micropores of <1 nm, especially the ultramicropores of <0.7 nm, resulting in the low fraction of ultramicropores in porous carbon frameworks. Furthermore, these common chemical-activating agents are prone to destroy the morphology and structure of final porous carbons and usually trigger the tough requirements for equipment, which easily corrodes the equipment due to their high corrosion. Meanwhile, the removal of the residues from the products could bring environmental pollution problems.[26] These issues seriously restrict their large-scale industrial application. Consequently, it is greatly desirable to explore a mild activating agent with environmental friendliness for rationally tailoring ultramicropore size in highly effective CO_2 capture.

In addition, different kinds of carbon sources have been employed to synthesize porous carbons, and importantly, precursors play an important role in engineering morphology and porosity. Owing to its low cost, diversity, and renewability, biomass is a widely available precursor to synthesize porous carbons for different applications.[27−30] In this work, we developed an efficient and low-cost strategy for the synthesis of microporous carbons using $CuCl_2$ as a dynamic porogen and wasted natural woods as carbon precursors. This strategy highlights to construct microporous carbons with a tunable narrow micropore structure by varying the concentration of the $CuCl_2$-activating agent, particularly in ultramicropores of <0.7 nm. As expected, the resultant microporous carbons exhibit tailorable microporosity, especially a high fraction of ultramicropores (<0.7 nm) and supermicropores ranging from 1.0 to 1.5 nm, and a suitable surface nitrogen group by a self-doping process. Benefiting from these key characteristics, these as-prepared microporous carbons obtain a satisfactory CO_2 adsorption capacity, moderate adsorption heat, and superior CO_2/N_2 selectivity and reusability for CO_2 capture at ambient conditions. Importantly, our developed strategy shows great potential for producing sustainable porous carbon-based adsorbents for highly efficient CO_2 capture from postcombustion flue gases in a one-stone-to-bird manner.

2. EXPERIMENTAL SECTION

2.1. Chemicals. Anhydrous copper chloride ($CuCl_2$) and hydrochloric acid solution (HCl) were purchased from Shanghai Aladdin Industrial Corporation. All of the chemicals are of analytical grade and used without further purification.

2.2. Preparation of Sustainable Microporous Carbons. Waste *paulownia* wood was collected and cut into powder, washed repeatedly with deionized water, and then immersed in ethanol for 12 h. Subsequently, the powders were washed and dried at 70 °C overnight. Then, 4 g of dried powders was precarbonized at 400 °C for 2 h in an Ar atmosphere with a heating rate of 5 °C/min. The black powders were obtained and used as the carbon precursor.

Microporous carbons were synthesized by an inorganic dynamic activation strategy using $CuCl_2$ as a porogen. Typically, 1 g of the obtained black powders was impregnated in 40 mL of $CuCl_2$ solution with a certain mass. After stirring for 4 h, the solution was evaporated to dryness on a rotary evaporator and the obtained powders were dried at 60 °C under vacuum. The dried powders were carbonized in a tubular furnace at 800 °C for 2 h under an Ar atmosphere with a heating rate of 5 °C/min and an Ar flow rate of 50 mL/min. The carbonized products were immersed in HCl solution (2 M) overnight. Then, the products were filtered and washed with deionized water until the pH of the washed solution became neutral. Finally, the materials were dried at 70 °C to obtain microporous carbons, which were designated as MC-*x*, where *x* refers to the mass ratio of $CuCl_2$/precursor (x = 1, 2, 3, and 4).

2.3. Characterizations. X-ray diffraction (XRD) patterns were carried out by using a Bruker D8 diffractometer using Cu Kα radiation (λ = 0.15418 nm) as an X-ray source. Raman spectra were collected using a laser Raman spectrometer (Thermo Fisher Scientific, USA) equipped with a He−Ne laser wavelength of 532 nm. Fourier transform infrared (FTIR) spectra were measured on a Nicolet 6700 spectrometer. Pore structure characterization was determined from N_2 adsorption−desorption isotherms at −196 °C using Micromeritics ASAP 2020. Before adsorption, the samples were outgassed at 200 °C for 10 h. The specific surface area was calculated using the Brunauer−Emmett−Teller (BET) method, and the pore size distribution was calculated by density functional theory (DFT). The morphology was observed through scanning electron microscopy (SEM, JSM-IT300, JEOL, JPN) and transmission electron microscopy (TEM, Tecnai G^2 20 S-TWIN, USA). X-ray photoelectron spectra (XPS) were obtained on a K-Alpha plus X-ray photoelectron spectrometer with an exciting source of Al-Ka (1486.6 eV).

https://doi.org/10.1021/acsomega.3c05842
ACS Omega 2023, 8, 41641−41648

2.4. Gas Adsorption Measurements. Gas adsorption isotherms of CO_2 and N_2 at the desired temperatures were determined using a Micromeritics ASAP 2020 instrument. The samples were degassed at 200 °C for 10 h before each gas uptake measurement. The isotherms of CO_2 and N_2 at 0 and 25 °C were conducted in an ice−water bath and a water bath, respectively.

3. RESULTS AND DISCUSSION

3.1. Structural Analysis of MC-*x* Materials. Waste *paulownia* woods are usually discarded or incinerated, which cause serious environmental pollution and damage. The main components of waste natural woods are cellulose, hemicellulose, and lignin, which can act as the carbon source for the preparation of carbon-based materials. In this work, microporous carbons were prepared by a new dynamic activation strategy using waste natural woods as single carbon and nitrogen sources as well as $CuCl_2$ as a dynamic porogen. The fabrication process is illustrated in Figure 1a. First, the waste paulownia woods were crushed, washed, and dried. Then, the dried sawdust was precarbonized at 400 °C for 2 h under Ar and the obtained black powders were used as a precursor. Next, the obtained black powders were immersed in $CuCl_2$ solution with the different dosages for 4 h. After evaporation of water on a rotary evaporator, the dried mixture was heated under an Ar atmosphere at 800 °C for 2 h. Finally, the microporous carbons were obtained by being treated with acid to remove the generated Cu species during the heat treatment. During the heat treatment, the carbon skeleton was generated and reacted with $CuCl_2$ to etch the carbon skeleton. Under the dynamic pore-creating of $CuCl_2$, the evaporation and leaching of Cu can gradually generate developed hierarchical micropores.[31] Importantly, the hierarchical microporosity can be tailored by adjusting the concentration of $CuCl_2$.

To confirm the reasonability of the above proposed $CuCl_2$ dynamic activation process, the XRD pattern of the intermediate was recorded. After heat treatment at 800 °C and before acid washing, the characteristic diffraction peaks of metallic Cu (JCPDS no. 04-0836) can be observed (Figure 1b), which should be from the reduction of Cu^{2+} by carbon or reductive gases as carbonization and pyrolysis proceeded. Such results demonstrate that the proposed $CuCl_2$ dynamic activation mechanism described above is reasonable. Figure 1c shows the XRD patterns of the MC-*x* samples. Two wide diffraction peaks at around $2\theta = 24$ and 43° are presented in all MC-*x* samples, which correspond to the (002) and (100) planes of graphitic carbon. However, the weak diffraction intensity suggests the low degree of crystallinity, indicative of the amorphous carbon framework in MC-*x*. The graphitization degree and carbon defect of MC-*x* were further examined by Raman spectra (Figure 1d). Obviously, two intensive peaks located at ∼1356 and 1586 cm^{-1} can be found in all MC-*x* samples, which are, respectively, assigned to the D- and G-bands. The D-band reflects the disordered carbon structure caused by carbon lattice defects, and the G-band corresponds to the ordered alignment of graphitic carbon structure.[32] Furthermore, the relative intensity of D- and G-bands (I_D/I_G) can be used to evaluate the graphitization degree and defect density of the carbon skeleton. The corresponding I_D/I_G values of MC-1, MC-2, MC-3, and MC-4 are 1.14, 1.12, 1.05, and 1.02, respectively. Such results reveal that the resultant MC-*x* materials have a low graphitization level and a high defect density. However, with the increase of $CuCl_2$ dosage, the graphitization degree of the carbon microstructure is enhanced, which could be related to the catalytic effect of metallic Cu species to the carbon skeleton.

Electron microscopy technology was employed to reveal the evolution of the microstructure and morphology. As shown in the SEM image of the original precarbonized precursor (Figure S1, Supporting Information), a regular microchannel structure arrayed in parallel with an average tube diameter of about 5 μm can be clearly observed and the tube surface is smooth with the ignorable pores. After $CuCl_2$ activation, all MC-*x* samples basically inherit the original aligned microchannel structure (Figure 2a−d). However, it can be clearly observed that the surface roughness of MC-*x* gradually enhances with the etching of $CuCl_2$ porogen and even some small fragments can be found. Meanwhile, some macropores can be observed on the surface of microtubes and the number of pores increases with the enhancement of $CuCl_2$ dosage. Such results should be ascribed to the removal of reduced Cu nanoparticles by acid washing that contributes these macropores on the surface of MC-*x* samples. Furthermore, large numbers of irregular white spots can be clearly observed in the high-magnification TEM images (Figure 2e,f) and the number of micropores enhances with the increase of the $CuCl_2$ dosage. Such results further confirm that the $CuCl_2$ dynamic porogen can etch the carbon skeleton to generate abundant micropores and even small mesopores. Importantly, the amount and size of these nanopores can be tailored by adjusting the $CuCl_2$ dosage.

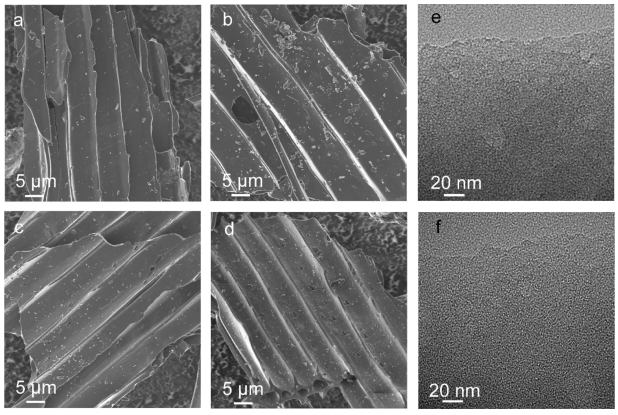

Figure 2. Structure and morphology characterizations. SEM images of (a) MC-1, (b) MC-2, (c) MC-3, and (d) MC-4. TEM images of (e) MC-2 and (f) MC-3.

The N_2 physisorption technology was employed to further explore the porosity of the as-prepared MC-*x* samples. Microporous carbon synthesized from waste paulownia wood without $CuCl_2$ treatment exhibits a typical type I isotherm of microporous material with a relative low surface area of 360.7 $m^2\ g^{-1}$ and a narrow pore size distribution of 0.6−1.5 nm (Figure S2). Obviously, all MC-*x* samples exhibit a typical type I isotherm (Figure 3a), indicative of the microporous structure from $CuCl_2$ dynamic activation. The sharp adsorption inflection at low relative pressure of <0.01 reflects a superior microporosity, and the higher N_2 adsorption amount means a larger micropore surface area. As a result, an improved micropore surface area is obtained with an increase of the $CuCl_2$ dosage (Table 1), which should be attributed to the progressive $CuCl_2$ dynamic activation. The evolution of the hierarchical porosity can be further analyzed by the pore size

https://doi.org/10.1021/acsomega.3c05842
ACS Omega 2023, 8, 41641−41648

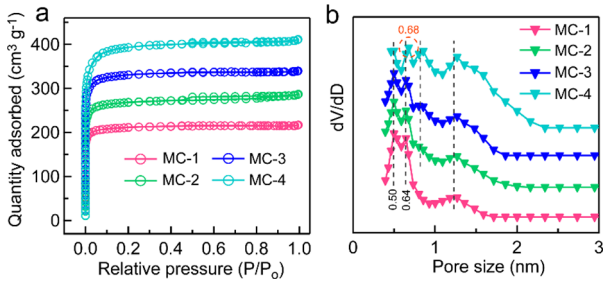

Figure 3. Pore structure analysis. (a) N_2 adsorption−desorption isotherms and (b) pore size distribution of MC-*x* samples.

distribution (Figure 3b). Apparently, all MC-*x* samples show prominent microporosity with a multiscale micropore size and the micropore size and proportion stepwise vary with enhancement of the $CuCl_2$ dosage. The micropores of MC-1 mainly center at 0.50 and 0.64 nm as well as at 1.21 nm, but the micropore of 1.21 nm is a negligible proportion in its porosity. Except the 0.5 and 0.64 nm micropores, an additional micropore of 0.82 nm can be generated in MC-2 and MC-3 and the proportion of 0.82 nm is larger in MC-3. Compared with MC-1, the 1.21 nm micropore is stepwise widened to 1.23 nm (MC-2) and 1.25 nm (MC-3) and the proportion of this micropore is gradually increased. Noticeably, the micropores of 0.50 and 0.64 nm are dominant in MC-1, MC-2, and MC-3. Different from other MC-*x* samples, a widened micropore size is formed in MC-4 and its micropores center at 0.50, 0.68, 0.86, and 1.27 nm, and the proportions of 0.86 and 1.27 nm are apparently improved. Furthermore, additional micropores centered at 1.48−1.57 nm can be found in MC-4. Based on the above analysis result, it can be concluded that the $CuCl_2$ concentration plays a crucial role in tailoring the microporosity. With the increase of $CuCl_2$ concentration, the proportion of narrow micropores decreases and the micropore size gradually widens.

The surface chemistry environment of all of the as-obtained materials was first confirmed by FTIR analysis. As shown in Figure 4a, the hydrothermal precursor contains abundant surface functional groups, including C−C, C = C, C−OH, C−O−C, C−H, or N−H groups,[33] suggesting the presence of numerous oxygen-containing groups. After carbonization and $CuCl_2$ activation, all MC-*x* samples show a similar FTIR spectrum with few absorption bands and only C−C and C = C characteristic absorption peaks can be found (Figure 4b), which manifests the formation of a carbon skeleton with relatively high carbonization. XPS characterization was conducted to further study the surface chemical composition and functional groups of MC-*x*. The XPS spectrum of the hydrothermal precursor demonstrates the existence of C, N, and O elements (Figure S3), and a high O content is obtained, which is consistent with the analysis result of the FTIR spectrum. The survey spectra of MC-*x* reveal the composition of C, N, and O elements (Figure 4c), and their atomic concentrations are listed in Table S1, which evidently shows that the O contents in MC-*x* have a significant dependency on the $CuCl_2$ dosage. Such results should be related to the further elimination of surface oxygen-containing functional groups with the aid of $CuCl_2$ etching. Figure 4d presents the high-resolution O 1s spectra of MC-*x* samples. It can be deconvoluted into three separate peaks at ∼531.1, 532.1, and 533.1 eV, which are assigned to C═O or COOH groups, C−O or C−O-R groups, and O═C−O functional groups, respectively.[34,35] The N 1s spectra can be fitted into four peaks located at ∼397.9, 398.8, 399.8, and 402.7 eV (Figure 4e), which confirms that the main N species are pyridinic-N (N-6), pyrrolic-N (N-5), quaternary-N (N-Q), and pyridine-N-oxide (N-X), respectively.[36,37] Apparently, pyridinic-N and pyrrolic-N are dominant in surface N functional groups of MC-*x*, which could be conducive to the improvement of CO_2 capture capacity because of the relatively high basicity.[38]

3.2. CO_2 Capture Property of MC-*x* Materials.

Considering the prominent hierarchical micropores, high surface area, and suitable surface groups, the resultant MC-*x* materials are expected to be an ideal adsorbent for CO_2 capture. The CO_2 capture property of all MC-*x* samples is investigated at two representative temperatures of 273 and 298 K. As depicted in Figure 5a,b, the CO_2 uptakes of MC-*x* samples increase with the pressure at both temperatures, which manifests that a higher CO_2 uptake capacity could be obtained by rising the pressure. Furthermore, all MC-*x* samples exhibit a superior CO_2 uptake at 273 K than those at 298 K, manifesting that this CO_2 adsorption is an exothermic physical adsorption process.[39] The CO_2 uptakes of MC-*x* samples under 0.15 and 1.0 bar at 273 and 298 K are listed in Table S2. MC-3 shows the highest CO_2 uptakes of 5.31 and 1.81 mmol g^{-1} under 1.0 and 0.15 bar at 273 K, which is comparable and even higher than other porous carbon-based CO_2 adsorbents (Table S3). Such satisfactory CO_2 uptakes should be ascribed to its developed hierarchical micropores, especially the high-proportioned ultramicropores. Although MC-4 has the largest micropore surface area and pore volume, it exhibits a decreased rate of CO_2 uptake. Such result could be resulted from its high proportion of large micropores. Noticeably, MC-1 and MC-2 display higher CO_2 uptakes at 298 K under 0.15 and 1.0 bar and MC-1 exhibits the highest CO_2 uptake under below 0.3 bar. Based on the above results, it can be concluded that narrow micropores could make more contributions to CO_2 adsorption at low pressure and high temperature and large micropores could play a determined role in CO_2 adsorption at high pressure and low temperature. Such adsorption behaviors further certify the pore-filling mechanism during CO_2 capture

Table 1. Pore Textural Parameters of the MC-*x* Materials

sample	S_{BET} [a] (m^2 g^{-1})	S_{micro} [b] (m^2 g^{-1})	S_{ultra} [c] (m^2 g^{-1})	V_{total} [d] (cm^3 g^{-1})	V_{micro} [e] (cm^3 g^{-1})	V_{ultra} [f] (cm^3 g^{-1})	I_D/I_G	yield (%)
MC-1	841.4	814.6	335.7	0.34	0.32	0.10	1.14	49.6
MC-2	1065.7	1026.8	339.8	0.44	0.40	0.11	1.12	43.6
MC-3	1302.4	1252.8	328.1	0.46	0.43	0.09	1.05	39.8
MC-4	1538.2	1476.9	267.4	0.63	0.58	0.08	1.02	36.7

[a]BET surface area. [b]Micropore surface area calculated using the *V*−*t* plot method. [c]Ultramicropore surface area calculated using the DFT method to experimental CO_2 adsorption at 0 °C. [d]The total pore volume calculated by single-point adsorption at P/P_o = 0.9945. [e]The micropore volume calculated using the *V*−*t* plot method. [f]Ultramicropore volume calculated using the DFT method to experimental CO_2 adsorption at 0 °C.

https://doi.org/10.1021/acsomega.3c05842
ACS Omega 2023, 8, 41641−41648

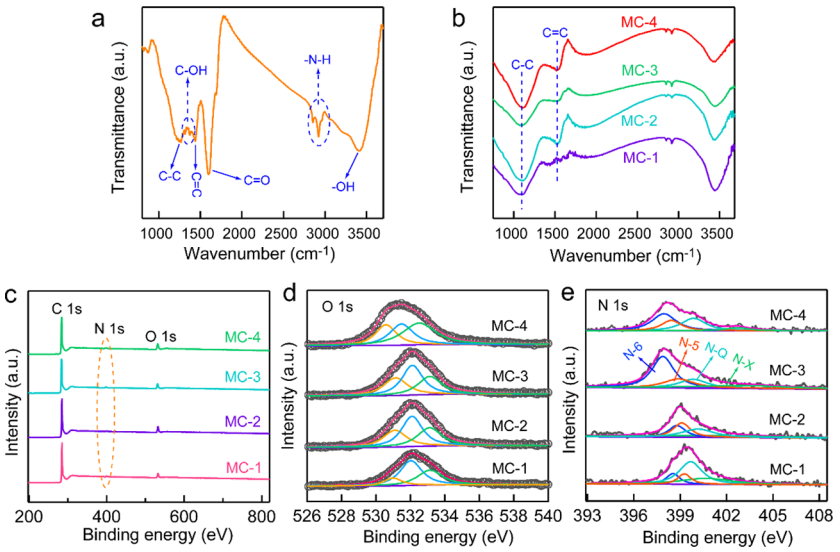

Figure 4. Surface chemistry analysis. FTIR spectra of the hydrothermal precursor (a) and MC-*x* samples (b). The XPS analysis of MC-*x*: (c) survey spectra and (d) O 1s and (e) N 1s (e) spectra.

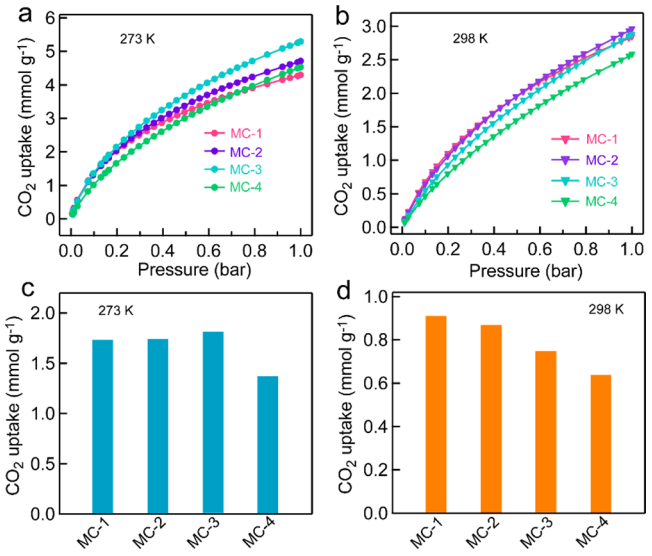

Figure 5. CO_2 capture capacity of MC-*x* at different adsorption conditions. (a) CO_2 adsorption isotherms at 273 (a) and 298 K (b). CO_2 uptakes under 0.15 bar at 273 K (c) and 298 K (d).

over porous carbon-based adsorbents.[40] To further analyze the influence of pore structure on the CO_2 capture behavior, the relationship between the porosity and CO_2 capture is summarized. As shown in Figure S4a−d, almost no correlation between CO_2 uptakes and total BET surface area, total pore volume, micropore surface area, and micropore pore volume are obtained. However, a good correlation between CO_2 uptakes and ultramicropore surface area/ultramicropore volume can be found (Figure S4e,f), which confirms the decisive role of ultramicropores of less than 0.7 nm on CO_2 capture capacity.

The flue gases from fossil fuel-fired power plant contain large numbers of CO_2, and the practical pressure of CO_2 in flue gases is about 0.15 bar.[41] As a result, the CO_2 capture capacity at 0.15 bar reflects the possibility of acting as a promising adsorbent for flue gases in practical application. Apparently, the variation trend of CO_2 uptakes at 0.15 bar is different from that at 1 bar (Figure 5c,d), especially for the uptakes at 298 K. MC-1 exhibits a highest CO_2 uptake, which further confirms the determined role of ultramicrpores on CO_2 capture behavior at low pressure and high temperature.

Except for the satisfactory CO_2 uptake, good selectivity is another vital demand for meeting the practical industrial application of multicomponent adsorption of CO_2. In general, the postcombustion flue gases contain a large number of N_2 and the proportion of N_2 is ∼73−77% in volume.[42] As a result, the selectivity of MC-*x* samples for CO_2 over N_2 in binary gas mixtures was evaluated using single-component isotherms. The CO_2 and N_2 adsorption isotherms of representative MC-2 and MC-3 at 273 and 298 K are presented in Figure 6a and b, respectively. The ideal adsorbed solution theory (IAST) method is employed to analyze the CO_2/N_2 selectivity (the calculated details are shown in the Supporting Information), which is a traditional and well-established way to predict the

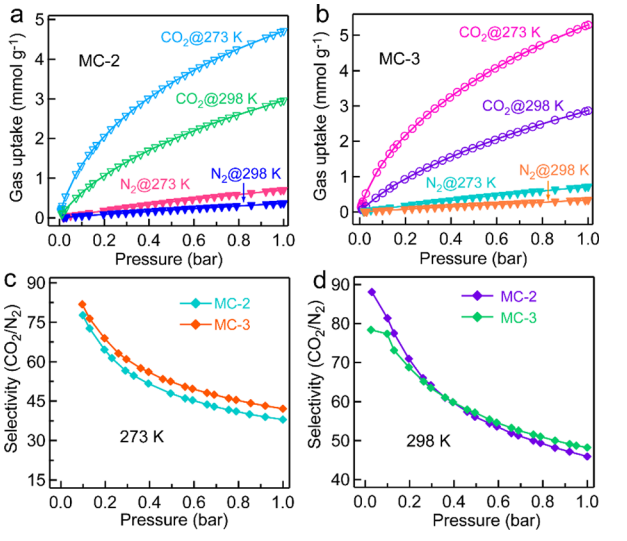

Figure 6. CO_2/N_2 adsorption selectivity. CO_2 and N_2 adsorption isotherms at 273 and 298 K over MC-2 (a) and MC-3 (b). IAST selectivity of CO_2/N_2 on MC-2 and MC-3 at 273 (c) and 298 K (d).

https://doi.org/10.1021/acsomega.3c05842
ACS Omega 2023, 8, 41641−41648

selectivity of adsorbents in a binary gas mixture. The CO_2/N_2 ratio is 15/85 (v/v) in the calculation of IAST selectivity, representing the practical composition of the flue gases. The CO_2/N_2 IAST selectivity of MC-3 at 273 K is higher than that of MC-2 (Figure 6c). The CO_2/N_2 IAST selectivity of MC-3 at 273 K is in the range of 82−42. The CO_2/N_2 selectivity shows a distinct decrease in the low-pressure region and finally achieves a plateau with a rise of pressure. The selectivity of MC-3 still reaches 42 at 1 bar and 273 K. Notably, MC-2 exhibits a higher CO_2/N_2 selectivity at 298 K in the low-pressure region below 0.4 bar (Figure 6d), which results in a higher CO_2 uptake at 0.15 bar and 298 K. Such results further confirm the dominant contribution of ultramicropores on CO_2 capture at low pressure and high temperature. The CO_2/N_2 IAST selectivity of MC-2 is 78 at 0.15 bar and 298 K and still keeps 48 at 1.0 bar and 298 K, which is comparable or even much higher than those of most of reported porous carbonaceous adsorbents.[43−46] Importantly, the CO_2/N_2 selectivity of MC-*x* at 298 K has no decrease and even shows an increase, which significantly favors the practical application in capturing CO_2 from the flue gases.

The CO_2/N_2 selectivity of MC-*x* is also evaluated based on Henry's law using the ratio of the initial slope of the CO_2 and N_2 adsorption isotherms. The initial slopes of the CO_2 and N_2 adsorption isotherms of MC-2 and MC-3 at 273 and 298 K are shown in Figure 7, and the corresponding equations are

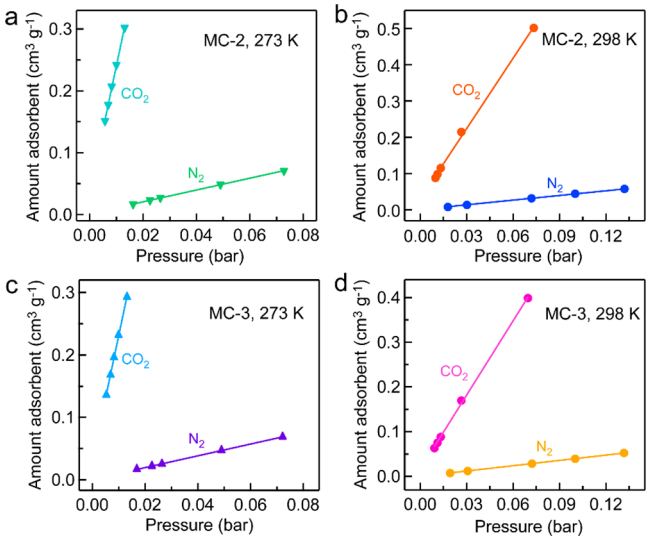

Figure 7. Initial slope calculated from CO_2 and N_2 isotherms. (a) MC-2 at 273 K. (b) MC-2 at 298 K. (c) MC-3 at 273 K. (d) MC-3 at 298 K.

summarized in the Supporting Information. The Henry's law CO_2/N_2 selectivities of MC-2 (MC-3) are 21 (22) and 15 (14) at 273 and 298 K, respectively. It is obvious that the Henry's law CO_2/N_2 selectivity is lower than that of IAST selectivity, which could be related to the different fitted models in the two calculation methods or the heterogeneity of surface adsorption sites. However, the tendency in CO_2/N_2 selectivity measured by the IAST and Henry's law is consistent. According to the above analysis results, it can be concluded that the good CO_2/N_2 selectivity should be related to the proportion of the ultramicropore and pore size.

The surface interaction strength between MC-*x* adsorbents and CO_2 molecules was examined by the isosteric heat of adsorption calculated from the isotherms at 273 and 298 K using the Clausius−Clapeyron equation.[15] As displayed in Figure 8a, the initial Q_{st} values of MC-*x* are in the range 36−30

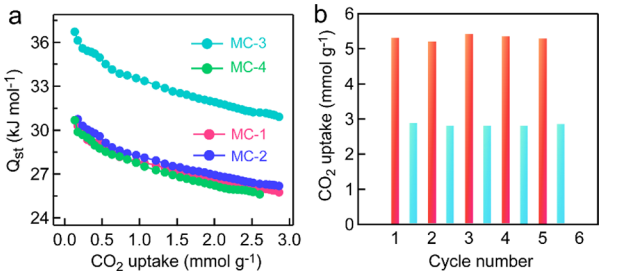

Figure 8. (a) Isosteric heat of CO_2 adsorption on MC-*x* samples calculated from the adsorption isotherms at 273 and 298 K. (b) Recycling stability test of MC-3.

kJ mol^{-1} at nearly zero CO_2 loading. Such Q_{st} values are much lower than the level of chemisorption, which indicates that the CO_2 adsorption process over MC-*x* is mostly dominated by the physical adsorption. Furthermore, it can be noticed that the total Q_{st} values of MC-*x* are a little higher than those of pure carbon-based CO_2 adsorbents and the improved Q_{st} values could benefit from the presence of a weak intermolecular interaction contributed from surface nitrogen-containing groups. Obviously, all the Q_{st} of MC-*x* show a sharp decrease at low CO_2 surface coverage, which is ascribed to the continuous occupancy of the adsorption sites. The Q_{st} values decrease with the increase in the level of CO_2 uptake, suggesting the heterogeneity of adsorption sites on the MC-*x* adsorbents. MC-3 shows a higher Q_{st}, which should benefit from its superior hierarchical porosity, high-proportioned microporosity, and suitable surface nitrogen content. As a promising CO_2 adsorbent, the superior recyclability and regeneration with low energy consumption are essential for practical application. The stability test of representative MC-3 was performed in five consecutive cycles at 273 and 298 K (Figure 8b). For the stability test, the recycled MC-3 adsorbent was degassed at room temperature for 2 h for the next cycle of CO_2 adsorption. There was almost no change in CO_2 uptake after five successive cycles, manifesting the prominent reusability of MC-3 with low energy requirement. Given the superior CO_2 uptake, moderate Q_{st}, satisfactory CO_2/N_2 selectivity, and easy regeneration, the resultant MC-*x* materials are believed to be highly promising adsorbents for CO_2 capture from the flue gases in the pressure swing adsorption technology.

4. CONCLUSIONS

In summary, we designed a series of microporous carbons with tunable hierarchical microporosity and surface chemistry properties by using a novel dynamic porogen of $CuCl_2$ and biowaste as carbon sources. Innovatively, the hierarchical microporosity can be easily tailored by varying the dosage of the $CuCl_2$ porogen, especially the ultramicropore region centered primarily at pore sizes of 0.4−0.8 nm. The surface chemistry environment can be modified by self-doping from the carbon precursor. The well-developed microporosity, especially the high-proportioned microporosity of less than 1 nm, and surface self-doped nitrogen species favor the as-obtained MC-*x* materials in highly effective capturing of CO_2. Based on the analysis of CO_2 capture behaviors, the resultant

https://doi.org/10.1021/acsomega.3c05842
ACS Omega 2023, 8, 41641−41648

MC-x materials exhibit satisfactory CO_2 adsorption capacity, moderate Q_{st}, high CO_2/N_2 selectivity, and superior regeneration ability, which are believed to be the promising adsorbents for CO_2 capture from flue gases in practical application. Importantly, we develop an almost zero-cost and industrially friendly route to convert biowaste to high-added-value products, which not only relieves the environmental pollution caused by biowaste but also obtains high-performance porous carbon-based CO_2 adsorbents.

■ ASSOCIATED CONTENT

Supporting Information

The Supporting Information is available free of charge at https://pubs.acs.org/doi/10.1021/acsomega.3c05842.

SEM image of the pre-carbonized precursor at 400 °C; adsorption−desorption isotherm and pore size of microporous carbon synthesized from waste paulownia wood without $CuCl_2$ treatment; XPS spectrum of the pre-carbonized precursor at 400 °C; the relationships between CO_2 uptakes at 298 K under 1.0 bar and different pore parameters; elemental and XPS analyses of the MC-x materials; the CO_2 uptakes of the MC-x materials at different temperatures and pressures; comparison of the CO_2 adsorption capacity over different carbon-based adsorbents; ideal adsorbed solution theory; and Henry's law selectivity (PDF)

■ AUTHOR INFORMATION

Corresponding Authors

Li Dai − *College of Forestry, Henan Agricultural University, Zhengzhou, Henan 45002, China*; Email: 13937182216@163.com

Yanmei Wang − *College of Forestry, Henan Agricultural University, Zhengzhou, Henan 45002, China*; orcid.org/0000-0002-8837-3586; Email: wym3554710@163.com

Authors

Shunyang Yao − *College of Forestry, Henan Agricultural University, Zhengzhou, Henan 45002, China*

Zhi Li − *College of Forestry, Henan Agricultural University, Zhengzhou, Henan 45002, China*; orcid.org/0000-0001-5612-9477

Zhen Liu − *College of Forestry, Henan Agricultural University, Zhengzhou, Henan 45002, China*

Xiaodong Geng − *College of Forestry, Henan Agricultural University, Zhengzhou, Henan 45002, China*

Complete contact information is available at: https://pubs.acs.org/10.1021/acsomega.3c05842

Author Contributions

#S.Y. and Z.L. contributed equally to this work.

Notes

The authors declare no competing financial interest.

■ ACKNOWLEDGMENTS

This work was supported by Henan Agricultural University (30400376). We would like to thank Tianxiao Ma from the College of Forestry, Xinyang Agricultural and Forestry University, for his support of this experiment.

■ REFERENCES

(1) Singh, G.; Lee, J.; Karakoti, A.; Bahadur, R.; Yi, J. B.; Zhao, D. Y.; AlBahily, K.; Vinu, A. Emerging trends in porous materials for CO_2 capture and conversion. *Chem. Soc. Rev.* **2020**, *49*, 4360−4404.

(2) Fu, D. L.; Park, Y.; Davis, M. E. Confinement effects facilitate low-concentration carbon dioxide capture with zeolites. *Proc. Natl. Acad. Sci. U.S.A.* **2022**, *119*, No. e2211544119.

(3) Heldebrant, D. J.; Kothandaraman, J.; Dowell, N. M.; Brickett, L. Next steps for solvent-based CO_2 capture; integration of capture, conversion, and mineralisation. *Chem. Sci.* **2022**, *13*, 6445−6456.

(4) Aghel, B.; Behaein, S.; Alobiad, F. CO_2 capture from biogas by biomass-based adsorbents: A review. *Fuel* **2022**, *326*, No. 125276.

(5) Wang, Q.; Pfeiffer, H.; Amal, R.; O'Hare, D. Introduction to CO_2 capture, utilization and storage (CCUS). *React. Chem. Eng.* **2022**, *7*, 487−489.

(6) Tome, L. C.; Marrucho, I. M. Ionic liquid-based materials: a platform to design engineered CO_2 separation membranes. *Chem. Soc. Rev.* **2016**, *45*, 2785−2824.

(7) Ding, M. L.; Liu, X.; Ma, P.; Yao, J. F. Porous materials for capture and catalytic conversion of CO_2 at low concentration. *Coordin. Chem. Rev.* **2022**, *465*, No. 214576.

(8) Oschatz, M.; Antonietti, M. A search for selectivity to enable CO2 capture with porous adsorbents. *Energy Environ. Sci.* **2018**, *11*, 57−70.

(9) Liu, R. S.; Shi, X. D.; Wang, C. T.; Gao, Y. Z.; Xu, S.; Hao, G. P.; Chen, S. Y.; Lu, A. H. Advances in post-combustion CO_2 capture by physical adsorption: From materials innovation to separation practice. *ChemSusChem* **2021**, *14*, 1428−1471.

(10) Shen, Y. F. Preparation of renewable porous carbons for CO_2 capture − A review. *Fuel Process. Technol.* **2022**, *236*, No. 107437.

(11) Zhang, Z.; Cano, Z. P.; Luo, D.; Dou, H. Z.; Yu, A. P.; Chen, Z. W. Rational design of tailored porous carbon-based materials for CO_2 capture. *J. Mater. Chem. A* **2019**, *7*, 20985−21003.

(12) Shi, W. W.; Yu, J.; Liu, H. L.; Gao, D. F.; Yuan, A. L.; Chang, B. B. Hierarchically nanoporous carbon for CO_2 capture and separation: roles of morphology, porosity, and surface chemistry. *ACS Appl. Nano Mater.* **2023**, *6*, 7887−7900.

(13) Gao, X. Y.; Yang, S. T.; Hu, L. F.; Cai, S. Y.; Wu, L. Q.; Kawi, S. Carbonaceous materials as adsorbents for CO_2 capture: synthesis and modification. *Carbon Capture Sci. & Technol.* **2022**, *3*, No. 100039.

(14) Chang, B. B.; Shi, W. W.; Yin, H.; Zhang, S. R.; Yang, B. C. Poplar catkin-derived self-templated synthesis of N-doped hierarchical porous carbon microtubes for effective CO_2 capture. *Chem. Eng. J.* **2019**, *358*, 1507−1518.

(15) Hao, G. P.; Li, W. C.; Qian, D.; Wang, G. H.; Zhang, W. P.; Zhang, T.; Wang, A. Q.; Schuth, F.; Bongard, H. J.; Lu, A. H. Structurally designed synthesis of mechanically stable poly-(benzoxazine-co-resol)-based porous carbon monoliths and their application as high-performance CO_2 capture sorbents. *J. Am. Chem. Soc.* **2011**, *133*, 11378−11388.

(16) Zhang, Y. F.; Shi, W. W.; Zhang, S. R.; Zhao, S.; Yang, B. C.; Chang, B. B. Rational design of β-cyclodextrins-derived hierarchically porous carbons for CO_2 capture: The roles of surface chemistry and porosity on CO_2 capture. *J. CO2 Utilization* **2022**, *66*, No. 102244.

(17) Wickramaratne, N. P.; Jaroniec, M. Importance of small micropores in CO_2 capture by phenolic resin-based activated carbon spheres. *J. Mater. Chem. A* **2013**, *1*, 112−116.

(18) Wang, J. C.; Kaskel, S. KOH-activation of carbon-based materials for energy storage. *J. Mater. Chem.* **2012**, *22*, 23710−23725.

(19) Chang, B. B.; Guo, Y. Z.; Li, Y. C.; Yin, H.; Zhang, S. R.; Yang, B. C.; Dong, X. P. Graphitized hierarchical porous carbon nanospheres: simultaneous activation/graphitization and superior supercapacitance performance. *J. Mater. Chem. A* **2015**, *3*, 9565−9577.

(20) Hu, L. F.; Zhu, Q. Z.; Wu, Q.; Li, D. S.; An, Z. X.; Xu, B. Natural biomass-derived hierarchical porous carbon synthesized by an in situ hard template coupled with NaOH activation for ultrahigh rate supercapacitors. *ACS Sustainable Chem. Eng.* **2018**, *6*, 13949−13959.

(21) Kim, M. J.; Choi, S. W.; Kim, H.; Mun, S.; Lee, K. B. Simple synthesis of spent coffee ground-based microporous carbons using K_2CO_3 as an activation agent and their application to CO_2 capture. *Chem. Eng. J.* **2020**, *397*, No. 125404.
(22) Liyanaarachchi, H.; Thambiliyagodage, C.; Lokuge, H.; Vigneswaran, S. Kinetics and thermodynamics study of methylene blue adsorption to sucrose-and urea-derived nitrogen-enriched, hierarchically porous carbon activated by KOH and H_3PO4. *ACS Omega* **2023**, *8*, 16158−16173.
(23) Kiełbasa, K.; Bayar, Ş.; Varol, E. A.; Srenscek-Nazzal, J.; Bosacka, M.; Miadlicki, P.; Serafin, J.; Wrobel, R. J.; Michalkiewicz, B. Carbon dioxide adsorption over activated carbons produced from molasses using H_2SO_4, H_3PO_4, HCl, NaOH, and KOH as activating agents. *Molecules* **2022**, *27*, 7467.
(24) Silvestre-Albero, J.; Wahby, A.; Sepulveda-Escribano, A.; Martinez-Escandell, M.; Kaneko, K.; Rodriguez-Reinoso, F. Ultrahigh CO_2 adsorption capacity on carbon molecular sieves at room temperature. *Chem. Commun.* **2011**, *47*, 6840−6842.
(25) Yang, J.; Yue, L. M.; Hu, X.; Wang, L. L.; Zhao, Y. L.; Lin, Y. Y.; Sun, Y.; Dacosta, H.; Guo, L. P. Efficient CO_2 capture by porous carbons derived from coconut shell. *Energy Fuels* **2017**, *31*, 4287−4293.
(26) Yue, L. M.; Xia, Q. Z.; Wang, L. W.; Wang, L. L.; Dacosta, H.; Yang, J.; Hu, X. CO_2 adsorption at nitrogen-doped carbons prepared by K_2CO_3 activation of urea-modified coconut shell. *J. Colloid Interface Sci.* **2018**, *511*, 259−267.
(27) Sevilla, M.; Fuertes, A. B. Sustainable porous carbons with a superior performance for CO_2 capture. *Energy Environ. Sci.* **2011**, *4*, 1765−1771.
(28) González, A. S.; Plaza, M. G.; Rubiera, F.; Pevida, C. Sustainable biomass-based carbon adsorbents for post-combustion CO_2 capture. *Chem. Eng. J.* **2013**, *230*, 456−465.
(29) Singh, G.; Lakhi, K. S.; Sil, S.; Bhosale, S. V.; Kim, I.; Albahily, K.; Vinu, A. Biomass derived porous carbon for CO_2 capture. *Carbon* **2019**, *148*, 164−186.
(30) Quan, C.; Zhou, Y.; Wang, J.; Wu, C. F.; Gao, N. B. Biomass-based carbon materials for CO_2 capture: A review. *J. CO2 Utilization* **2023**, *68*, No. 102373.
(31) Shi, W. W.; Zhang, Q. Q.; Liu, S. J.; Su, S. S.; Chang, B. B.; Yang, B. C. Copper ions-assisted inorganic dynamic porogen of graphene-like multiscale microporous carbon nanosheets for effective carbon dioxide capture. *J. Colloid Interface Sci.* **2021**, *600*, 670−680.
(32) Wang, G.; Yang, J.; Park, J.; Guo, X. L.; Wang, B.; Liu, H.; Yao, J. Facile synthesis and characterization of graphene nanosheets. *J. Phys. Chem. C* **2008**, *112*, 8192−8195.
(33) Ren, S. H.; Deng, L. P.; Zhang, B.; Lei, Y. F.; Ren, H. Q.; Lv, J. X.; Zhao, R. J.; Chen, X. F. Effect of air oxidation on texture, surface properties and dye adsorption of wood-derived porous carbon materials. *Materials* **2019**, *12*, 1675.
(34) Wen, F.; Zhang, W.; Jian, W.; He, X.; Yin, J.; Shi, J.; Lin, H.; Lu, K.; Qin, Y.; Qiu, X. Sustainable production of lignin-derived porous carbons for high-voltage electrochemical capacitors. *Chem. Eng. Sci.* **2022**, *255*, No. 117672.
(35) Yin, L. H.; Hu, P. Y.; Liang, C.; Wang, J.; Li, M.; Qu, W. D. Construction of self-supporting ultra-micropores lignin-based carbon nanofibers with high areal desalination capacity. *Int. J. Biol. Macromol.* **2023**, *225*, 1415−1425.
(36) Chen, M. F.; Yu, D.; Zheng, X. Z.; Dong, X. P. Biomass based N-doped hierarchical porous carbon nanosheets for all-solid-state supercapacitors. *J. Energy Storage* **2019**, *21*, 105−112.
(37) Zhang, H. B.; Zhang, N.; Man, J. Z.; Du, Y. H.; Cui, J. L.; Sun, J. C. A sustainable approach from rice husks to P, N-dual doping porous C/SiO_x composites for high-performance lithium-ion battery anodes. *J. Electroanal. Chem.* **2022**, *904*, No. 115939.
(38) Xie, W. H.; Yao, X. Y.; Li, H.; Li, H. R.; He, L. N. Biomass-based N-rich porous carbon materials for CO_2 capture and in-situ conversion. *ChemSusChem* **2022**, *15*, No. e202201004.
(39) Ge, C.; Song, J.; Qin, Z.; Wang, J.; Fan, W. Polyurethane foam-based ultramicroporous carbons for CO_2 capture. *ACS Appl. Mater. Interfaces* **2016**, *8*, 18849−18859.
(40) Querejeta, N.; Gil, M. V.; Pevida, C.; Centeno, T. A. Standing out the key role of ultramicroporosity to tailor biomass-derived carbons for CO_2 capture. *J. CO2 Utilization* **2018**, *26*, 1−7.
(41) Lu, W. G.; Sculley, J. P.; Yuan, D. Q.; Krishna, R.; Wei, Z. W.; Zhou, H. C. Polyamine-tethered porous polymer networks for carbon dioxide capture from flue gas. *Angew. Chem., Int. Ed.* **2012**, *51*, 7480−7484.
(42) Liu, X.; Liu, J. J.; Sun, C. G.; Liu, H.; Wang, W. L.; Smith, E.; Jiang, L.; Chen, X. Y.; Snape, C. Design and development of 3D hierarchical ultra-microporous CO_2-sieving carbon architectures for potential flow-through CO_2 capture at typical practical flue gas temperatures. *J. Mater. Chem. A* **2020**, *8*, 17025−17035.
(43) Nandi, R.; Jha, M. K.; Guchhait, S. K.; Sutradhar, D.; Yadav, S. Impact of KOH activation on rice husk derived porous activated carbon for carbon capture at flue gas alike temperatures with high CO_2/N_2 selectivity. *ACS Omega* **2023**, *8*, 4802−4812.
(44) Wang, F.; Zeng, Y.; Hou, Y.; Cai, Q.; Liu, Q.; Shen, B.; Ma, X. CO_2 adsorption on N-doped porous biocarbon synthesized from biomass corncobs in simulated flue gas. *Langmuir* **2023**, *39*, 7566−7577.
(45) Jung, S. Y.; Lee, J. R.; Won, Y.; Lee, D. H.; Park, Y. C.; Bae, Y. S.; Kim, H. Hierarchical porous carbon beads for selective CO_2 capture. *J. CO2 Utilization* **2021**, *51*, No. 101659.
(46) Shao, L. S.; Sang, Y. F.; Huang, J. H. Imidazole-based hyper-cross-linked polymers derived porous carbons for CO_2 capture. *Microporous Mesoporous Mater.* **2019**, *275*, 131−138.

https://doi.org/10.1021/acsomega.3c05842
ACS Omega 2023, 8, 41641−41648